Journal of Geosciences and Geomatics, 2014, Vol. 2, No. 2, 62-75
Available online at http://pubs.sciepub.com/jgg/2/2/4

DOI:10.12691/jgg-2-2-4

Origin and Evolution of the Formation of the Cameroon Nyong Series in the Western Border of the Congo Craton

Ndema Mbongue J. L.[1,2], Ngnotue T.[3], Ngo Nlend C. D.[4], Nzenti J. P.[1,*], Cheo Suh E.[2]

[1]Laboratory of Petrology and Structural Geology, University of Yaoundé I, P.O. Box 3412, Cameroon
[2]Department of Geology, University of Buea, South West Region, P.O. Box 63 Buea, Cameroon
[3]Department of Geology, University of Dschang, West Region, P.O. Box. 67 Dschang, Cameroon
[4]Institute of Mineralogy and Geochemistry, University of Lausanne, Switzerland
*Corresponding author: jnzenti2010@gmail.com

Received April 22, 2014; Revised April 24, 2014; Accepted April 27, 2014

Abstract The Nyong series at Edéa and Eseka area is located in the western edge of the Congo Craton and comprise three distinguish rock units namely: metasedimentary rocks unit (schists, garnet-rich micaschist); meta-igneous rocks unit (pyroxene-rich gneiss, garnet-rich charnockitic gneiss, charnockitic gneiss, biotite-rich gneiss, amphibole and biotite-rich gneiss, garnet and amphibole-rich gneiss, amphibolite, pyribolite, pyrigarnite, garnet-rich amphibolite) and a unit of the rocks resulting from the melt (migmatite, TTG) displaying quartzo-feldspathic segregation arising from either in situ partial melting or injection along dykes or ductile shear zones. The meta-igneous rocks derived from (i) intermediate to basic tholeiitic rocks with high TiO_2 (0.6-3.47%) contents compatible with the extensive orogenic domain and (ii) calc-alkaline protolith display high FeO*/MgO (1.5-3.31) ratios which is in accordance with the typical domain of collisional orogeny. The chemical patterns of metasedimentary rocks are those of shale. The average Nb/Y (0.004) ratio and the fractioned REE patterns suggest that the contribution of alkaline vulcanite and a continental environment can be envisaged for these metasedimentary rocks.

Keywords: *nyong series, extensive orogenic domain, domain of collisional orogeny, shale, continental environment*

Cite This Article: Ndema Mbongue J. L., Ngnotue T., Ngo Nlend C. D., Nzenti J. P., and Cheo Suh E., "Origin and Evolution of the Formation of the Cameroon Nyong Series in the Western Border of the Congo Craton." *Journal of Geosciences and Geomatics*, vol. 2, no. 2 (2014): 62-75. doi: 10.12691/jgg-2-2-4.

1. Introduction

The Nyong series, one of the main block of the Congo Craton is situated in the western border of the Congo Craton in Cameroon [1,2]. The nature and the origin of the western of Congo Craton are not very well constrained. As a result, questions about the older events remain incompletely answered. To characterise the western border better, an area of 500 km^2 around Edéa and Eséka was mapped and petrologically and geochemically analyzed. The study area represents an Archean/Proterozoic lower crustal segment in which unaltered magmatic and metamorphic are well exposed. Because little data exist on the rock types in the western border of the Congo Craton, the main objectives of this study is to elucidate the nature, the origin, the geological significance and crustal evolution for a better understanding of the western border of the Congo Craton.

2. Geological Setting

The Congo craton is a large sub-circular mass of about 5711000 km^2 in area, and has a diameter of about 2500 km, comprising Archaean crust, early to mid-Proterozoic fold belt and Proterozoic cover [3]. Archaean formations form a ring of Archaean crusts of diverse sizes, (in clockwise succession from the south: Kasai–Angolan composite, Chaillu-Ntem complex, Gabon and Cameroon, Bouca, Bomu–Kibalian, Tanzania and Zambian), surrounding the unusually large, (1000–1200 km), sub-circular central late Proterozoic to Phanerozoic-filled Congo Basin [4]. The northwestern margin of the Archaean Congo craton in Southern Cameroon is represented by the Ntem complex [4,5,6], which is bordered in the north by the Yaoundé Group (e.g. [7,8,9,10]), of the Pan-African orogenic belt in Central Africa (Figure 1). The Ntem Complex is divided into two main structural domains: the Nyong series, to the northwest end, and the Ntem series, in the south-central area. The Ntem series is dominated by massive and banded plutonic rocks of the charnockite suite and by intrusive tonalites, trondhjemites and granodiorites. Some of these bodies were previously dated at ca. 2.9 Ga [2,11,12]. The igneous plutons contain large xenoliths of supracrustal rocks interpreted as remnants of greenstone belts and dated at ca. 3.1 Ga [13]. The studied areas, Edéa and Eséka (Figure 1 & Figure 2) belong to the Nyong series. This series consists of metasedimentary and metavolcanic rocks, as well as syn-to late-tectonic D_2

granitoids and syenites [1]; and displays three groups of ages [2,12,14,15]: (1) Archaean U-Pb ages (2500–2900 Ma) were obtained from detrital zircons in metasedimentary rocks, and presumably magmatic zircons in charnockites and migmatitic gneisses; (2) Palaeoproterozoic U-Pb zircon ages of ca. 2050 Ma corresponding to a thermometamorphic event associated with an important crustal melting and emplacement of some granite and syenite massifs, and (3) a Neoproterozoic U-Pb zircon age of 626 ± 26 Ma corresponding to the metamorphic effect of Pan-African thrusting. This unit includes some Archaean parts of the Ntem Complex that were reworked during a Palaeoproterozoic event, and new Palaeoproterozoic material that was accreted to the Archaean craton.

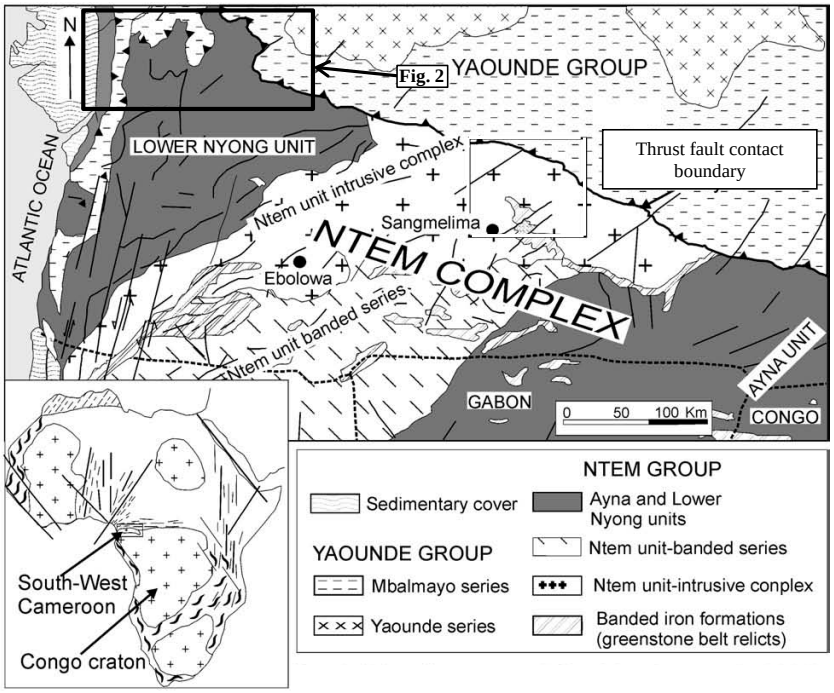

Figure 1. Geological map of south-west Cameroon after Maurizot et al. [2], modified by Shang et al. [3] showing the studied areas (Edéa and Eséka)

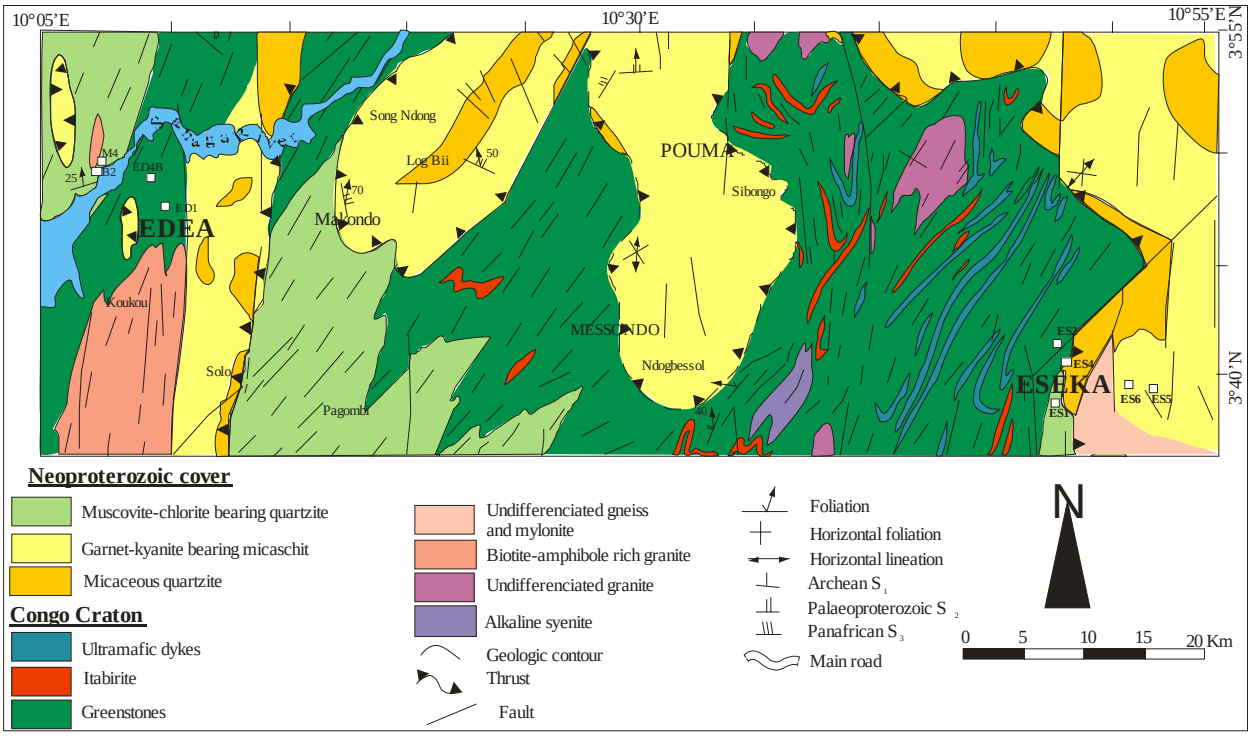

Figure 2. Geological map of Edéa and Eséka areas, modified from [2]

3. Analytical Methods

Fresh rock samples were collected from which more than 50 thin sections of metasediments, meta-igneous and migmatite were prepared and petrographically investigated. 52 representative samples (34 from Edéa, 18 from Eséka) were selected for chemical analysis. Major elements were analysed by inductively coupled plasma atomic emission spectrometry (ICP-AES), and trace

element by inductively coupled plasma mass spectrometry (ICP-MS) on a VG-Plasma Quad STE ICP mass spectrometer at the Institute of Mineralogy and Geochemistry of the University of Lausanne in Switzerland. The samples were dissolved in a Teflon pressure bomb, using a 1:1 mixture of HF and $HClO_4$ at 180°C, and then taken up in HNO_3 solution with an internal standard. After dissolution in HF-$HClO_4$, the samples were taken up in a mixture of HNO_3, 6N HCL and HF and diluted. These solutions were measured within 24 hours after dilution, to prevent absorption of high field strength elements (HFSE) on the sample bottle. Analysis uncertainties are currently better than 1% for major elements and 5-10% for trace element concentrations. Analysis precision for rare earth elements is estimated at 5% for concentrations > 10 ppm and 10% when lower. Representative analyses of different rock types are given in Table 1, Table 2, Table 3 and Table 4. Geochemical data were computed and the different and discriminate diagrams in the various plots displayed in Figure 4 to Figure 7.

Table 1. Major (wt.%) and trace (ppm) element analyses of representative garnet-rich micaschist from Edéa area

Rock	Garnet-rich micaschist				
Samples	M4	M4+	M4++	M5	M5*
wt.%					
SiO_2	63.66	62.98	62.56	66.20	67.05
TiO_2	0.76	0.76	0.76	0.82	0.81
Al_2O_3	17.59	17.39	17.29	14.88	15.02
Fe_2O_3	8.21	8.13	8.10	7.57	7.53
MnO	0.15	0.14	0.14	0.12	0.12
MgO	2.40	2.38	2.37	2.17	2.15
CaO	1.19	1.17	1.18	1.59	1.58
Na_2O	1.56	1.57	1.55	1.62	1.62
K_2O	3.88	3.83	3.85	3.28	3.29
P_2O_5	0.08	0.09	0.09	0.05	0.05
LOI	0.00	1.34	1.59	0.77	0.88
Total	99.48	99.78	99.47	99.08	100.10
ppm					
As	1194.7	1190.1	1149.2	619.7	606.4
Ba	900.1	885.1	887.9	425.9	398.2
Be	13.2	16.2	15.1	5.9	6.8
Co	181.1	176.8	174.8	141.2	139.4
Cr	1370.1	1335.6	1306.4	1030.5	960.6
Cs	8649.1	8424.3	8267.9	6587.5	6614.5
Cu	230.9	169.6	159.6	90.3	106.9
Ga	666.7	685.0	634.8	436.2	437.3
Mo	4.2	4.1	4.2	3.8	3.8
Nb	6.7	6.3	5.2	6.5	6.3
Ni	445.5	460.2	430.0	202.0	193.1
Pb	170.8	177.4	174.9	72.6	69.2
Rb	2296.5	2282.2	2230.0	1681.2	1650.2
Sc	205.1	200.7	197.7	151.7	147.6
Sr	269.5	269.0	262.0	169.9	161.6
Ta	6.0	7.2	6.1	12.2	11.2
Th	14.7	15.1	15.0	13.1	11.4
U	40.2	40.4	40.4	40.2	40.7
V	1258.8	1265.4	1209.8	894.2	871.3
W	191.4	202.2	199.5	95.2	93.4
Y	1625.4	1677.2	1631.1	2270.6	1921.2
Zn	784.0	795.4	767.3	484.0	483.9
Zr	107.5	107.2	105.3	142.9	137.4
La	468.616	464.847	461.507	228.051	221.513
Ce	92.518	92.169	91.298	40.925	40.326
Pr	331.923	322.229	324.075	147.312	143.805
Nd	56.531	54.020	57.409	25.991	27.826
Sm	11.572	11.315	10.824	9.194	8.301
Eu	45.957	46.843	46.708	27.534	25.536
Gd	7.066	6.844	6.848	4.440	4.088
Tb	44.755	45.759	41.442	29.045	26.962
Dy	9.304	9.138	8.468	5.985	5.468
Hf	6.831	7.038	6.989	12.402	12.133
Ho	24.296	26.882	25.385	17.353	16.2803
Er	3.903	3.866	3.683	2.649	2.50767
Tm	24.612	27.455	25.895	18.448	17.126
Yb	3.707	3.646	4.029	2.802	2.411
Lu	39.187	41.379	42.439	57.159	46.8447
Σ REE	1170.779	1163.431	1156.998	629.290	601.129
(La/Yb)N	9.315	9.394	8.441	6.769	5.998
Eu/Eu*	23.703	24.826	25.301	20.446	20.100
Th/U	0.365	0.374	0.371	0.280	0.326
La/Th	31.973	30.776	30.777	19.450	17.410
La/Sc	2.285	2.316	2.334	1.500	1.503
Th/Sc	0.071	0.075	0.076	0.077	0.086

Table 2. Major (wt. %) and trace (ppm) element analyses of representative pyroxene-rich gneiss, garnet-richcharnockitic gneiss and biotite-rich gneiss from Edéa area

Rocks	Pyroxene-rich gneiss					Garnet- rich charnockitic gneiss							Biotite-rich gneiss	
Samples	ED1	ED1B	ED1C	ED3B	ED3E	ED1D	ED1A	ED3A	ED3C	ED4C	ED3D	ED4B	A4B	B1
Wt%														
SiO2	61.29	61.30	/	55.03	59.60	67.77	68.41	72.05	66.23	70.92	67.18	72.08	66.15	68.61
TiO2	0.76	0.57	/	0.35	0.57	0.60	0.47	0.22	0.17	0.59	0.31	0.27	0.89	0.23
Al2O3	16.75	16.36	/	16.84	17.33	15.40	16.38	12.17	13.76	13.99	15.62	14.05	15.31	16.45
Fe2O3	7.23	6.44	/	16.51	10.99	4.19	3.38	7.39	10.13	5.10	7.17	3.71	3.93	1.42
MnO	0.10	0.11	/	0.16	0.11	0.05	0.04	0.07	0.10	0.05	0.08	0.08	0.04	0.03
MgO	3.03	4.27	/	4.96	3.75	1.40	1.07	2.34	3.13	1.58	2.28	0.93	1.00	0.42
CaO	6.63	5.69	/	2.13	1.80	4.09	4.25	2.02	2.05	2.47	2.02	2.55	2.80	1.21
Na2O	3.91	3.89	/	3.30	3.82	4.05	4.38	2.82	3.12	2.82	4.11	2.96	3.10	3.35
K2O	0.46	0.98	/	0.91	1.97	1.26	1.26	0.50	0.64	2.32	1.36	2.31	4.86	7.15
P2O5	0.16	0.15	/	0.04	0.04	0.13	0.17	0.04	0.03	0.03	0.05	0.03	0.44	0.10
LOI	-0.09	0.37	/	-0.56	-0.16	0.40	0.42	-0.09	-0.34	0.42	-0.07	0.15	0.57	1.11
Total	100.24	100.12	/	99.67	99.82	99.35	100.22	99.54	99.03	100.28	100.12	99.11	99.10	100.07
ppm														
As	3.07	46.61	55.52	582.97	4.11	49.33	51.28	64.11	47.82	511.96	116.30	347.96	343.99	1898.07
Ba	27.62	46.47	108.17	223.24	314.51	91.50	99.40	154.55	131.53	193.57	220.98	251.72	4014.04	624.22
Be	2.28	3.42	5.57	11.99	3.32	4.34	5.29	8.34	7.01	7.78	26.10	6.15	7.27	47.98
Co	40.26	43.28	40.11	41.99	29.17	29.36	24.21	108.44	152.75	73.73	98.49	29.22	25.23	29.88
Cr	179.53	706.84	261.61	95.82	185.41	133.32	115.90	1535.40	2031.82	378.73	1392.42	169.81	65.68	132.93
Cs	711.85	1044.49	3005.43	1409.87	1.22	1597.20	1607.14	1064.23	940.13	4536.55	3755.09	4978.62	17646.10	10152.58
Cu	69.90	36.57	110.33	89.43	55.78	65.25	52.10	247.90	478.46	351.00	247.88	55.84	48.37	103.10
Ga	65.03	90.10	200.37	120.19	25.01	121.61	133.14	95.34	109.48	222.50	273.16	218.39	948.02	742.67
Mo	0.07	0.59	0.17	13.68	3.02	0.38	0.31	1.19	0.73	4.66	0.95	2.25	0.98	68.61
Nb	1.77	2.56	4.23	3.37	13.77	2.95	2.85	15.91	15.60	7.48	13.40	5.21	2.96	11.49
Ni	94.67	127.60	181.30	52.93	115.36	84.51	69.43	549.60	912.47	214.29	441.57	94.30	22.62	69.40
Pb	0.72	0.83	3.37	68.55	18.77	1.33	2.33	12.82	6.54	23.95	47.39	70.86	1954.84	254.95
Rb	773.30	728.31	1234.81	680.54	28.55	1075.51	1083.74	859.26	866.04	1030.14	1079.21	1108.35	4832.93	3155.47
Sc	28.31	31.65	34.54	89.85	21.63	24.74	21.75	103.72	130.59	42.83	97.75	46.31	29.81	50.67
Sr	12.83	14.99	33.06	156.81	291.84	19.21	20.77	100.51	128.85	31.83	97.92	88.32	104.25	124.53
Ta	0.53	2.20	0.68	1.46	0.92	1.38	0.65	1.00	2.19	3.75	6.00	2.13	0.62	2.70
Th	0.29	0.80	0.78	11.80	7.78	0.31	0.29	3.83	3.13	4.04	4.90	3.74	22.61	31.86
U	40.43	40.20	39.97	39.97	3.08	40.43	40.20	40.20	40.20	40.43	40.43	40.43	40.20	40.20
V	227.77	213.81	216.77	328.85	143.73	189.47	153.51	547.37	565.84	521.14	500.19	203.20	306.27	240.05
W	5.98	21.73	33.81	64.01	1.36	27.21	25.91	60.33	49.57	79.96	105.08	98.39	304.97	347.35
Y	225.85	283.03	1021.66	729.93	29.60	79.31	53.91	2424.50	2355.26	1921.94	826.64	768.34	7966.51	1268.37
Zn	145.48	163.25	196.72	256.50	100.54	153.13	125.84	255.02	277.38	267.69	269.42	170.12	203.80	352.19
Zr	4.88	7.95	19.45	71.40	158.65	22.40	15.24	15.22	11.82	42.62	36.85	22.88	44.53	77.86
La	52.00	80.97	205.05	427.18	28.03	164.95	181.16	275.15	230.03	297.25	393.84	420.29	7284.25	981.91
Ce	5.44	8.23	22.06	52.78	58.24	15.75	17.89	26.50	21.52	26.23	38.30	37.51	725.57	112.54
Pr	20.31	29.20	77.92	207.65	7.59	54.11	63.08	89.73	74.71	76.88	127.04	113.03	2307.39	377.89
Nd	3.77	5.06	12.67	38.10	30.55	8.01	9.02	15.02	16.25	9.57	20.97	16.35	237.97	54.71
Sm	1.62	1.95	2.67	7.52	6.54	2.35	2.10	5.48	5.05	4.32	6.32	4.72	17.65	8.89
Eu	3.05	3.80	9.06	32.40	1.78	5.47	6.27	16.00	20.00	5.79	20.01	14.36	99.13	35.91
Gd	0.38	0.41	1.14	4.20	5.82	0.69	0.77	2.71	3.51	0.73	3.11	2.15	7.40	4.03
Tb	2.52	2.96	5.91	26.07	0.82	3.45	4.10	18.65	22.43	4.69	17.83	14.88	27.52	23.00
Dy	0.46	0.51	1.14	4.96	5.31	0.69	0.64	3.76	4.32	1.12	3.37	2.99	3.81	3.70
Hf	0.17	0.32	0.79	5.88	3.99	0.90	0.57	1.01	1.88	2.23	2.57	1.29	2.07	7.25
Ho	1.32	1.44	2.88	13.75	1.08	1.84	1.78	10.16	11.88	3.28	9.02	8.60	8.13	10.20
Er	0.19	0.18	0.41	1.98	2.84	0.23	0.20	1.44	1.79	0.63	1.19	1.32	0.88	1.49
Tm	1.28	1.49	2.66	13.94	0.44	1.59	1.45	10.00	10.94	4.43	8.60	8.32	5.61	9.44
Yb	0.15	0.21	0.39	2.18	2.84	0.21	0.20	1.45	1.61	0.66	1.23	1.24	0.96	1.55
Lu	4.82	6.14	21.75	19.47	0.44	1.85	1.37	62.50	57.75	46.54	19.87	20.33	177.69	34.27
Σ REE	97.48	142.86	366.50	858.05	156.29	262.08	290.59	539.55	483.67	484.36	673.29	667.39	10906.03	1666.79
(La/Yb)N	234.21	263.46	353.48	132.44	6.67	534.16	598.12	128.47	96.79	302.36	216.72	229.17	5125.65	426.79
(Gd/Yb)N	2.07	1.60	2.36	1.56	1.66	2.69	3.03	1.52	1.77	0.89	2.05	1.41	6.25	2.10
(Ce/Sm)N	0.81	1.02	1.99	1.69	2.15	1.62	2.06	0.69	1.03	1.47	1.46	1.92	9.92	3.05
Eu/Eu*	11.85	12.98	15.86	17.61	0.88	13.09	15.12	9.78	14.52	9.96	13.78	13.77	26.50	18.34

Table 3. Major (wt.%) and trace (ppm) element analyses of representative amphibole and biotite-rich gneiss, charnockitic gneiss, pyribolite and amphibolite from Edéa area

Rocks	Amphibole and biotite-rich gneiss			Charnockitic gneiss					Pyribolite		Amphibolite				
Samples	B2	B3	B4	ED2A	ED2B	ED2D	ED2E	A3	N1	MA2	P1	P2	P3	P4	P5
Wt.%															
SiO2	49.13	52.59	53.36	67.76	67.96	69.66	73.94	70.31	48.41	49.83	56.11	49.10	50.65	47.03	45.48
TiO2	2.42	2.00	2.03	0.46	0.46	0.34	0.27	0.43	1.12	3.47	0.78	0.76	0.31	1.30	1.30
Al2O3	16.15	15.41	15.69	15.98	16.82	15.41	14.44	14.32	11.86	12.98	14.38	15.13	14.55	6.54	6.09
Fe2O3	11.58	11.47	10.69	3.89	3.21	2.49	1.59	3.08	11.83	16.25	9.88	12.12	11.02	17.63	17.55
MnO	0.13	0.12	0.11	0.05	0.02	0.03	0.02	0.04	0.12	0.22	0.17	0.16	0.19	0.23	0.25
MgO	3.85	3.71	3.29	1.27	1.03	1.20	0.70	0.89	12.23	4.90	6.37	8.10	10.11	15.70	15.78
CaO	6.26	5.23	4.89	4.95	4.44	7.02	5.39	3.11	9.52	8.19	7.50	10.42	8.95	10.15	10.13
Na2O	2.38	2.34	2.75	4.35	4.29	3.28	3.17	4.02	1.01	2.27	3.51	2.88	2.79	0.88	0.73
K2O	4.70	4.08	4.08	0.91	1.38	0.49	0.52	1.75	2.01	1.52	1.00	1.10	0.78	0.42	0.42
P2O5	1.67	1.41	1.44	0.17	0.15	0.13	0.09	0.17	0.59	0.39	0.14	0.06	0.04	0.07	0.07
LOI	0.80	0.74	0.75	0.19	0.33	0.12	0.12	0.95	1.29	0.22	0.24	0.31	0.53	0.14	1.20
Total	99.06	99.11	99.09	99.98	100.07	100.16	100.25	99.07	99.98	100.23	100.07	100.14	99.92	100.07	98.99
ppm															
As	/	1.22	1.49	18.33	30.79	2.99	0.32	171.73	1.29	1.00	0.89	9.23	1.75	9.29	0.75
Ba	962.30	763.50	2158.29	94.12	88.19	59.31	4.55	1148.94	1921.74	1501.11	164.95	485.77	2946.59	488.70	579.96
Be	37.55	27.78	6.83	5.61	4.09	3.07	0.32	10.09	7.53	5.34	1.49	3.57	6.77	4.18	2.59
Co	74.02	68.13	29.01	21.29	23.62	9.46	0.79	35.07	26.48	28.69	115.16	34.12	38.77	35.09	58.00
Cr	410.26	386.46	144.93	117.97	67.63	89.77	11.04	148.96	56.24	147.26	1311.19	159.42	201.92	161.04	547.41
Cs	93.27	93.37	1.35	927.21	2143.90	337.65	37.59	8465.08	14.93	0.28	0.09	2.94	1.81	3.17	0.33
Cu	22.16	32.55	28.86	57.09	39.64	6.86	0.69	197.03	33.59	27.89	89.55	72.81	37.70	69.78	178.45
Ga	78.57	78.98	97.70	85.25	138.72	42.49	4.24	394.11	89.62	79.63	17.23	44.57	124.92	45.32	42.17
Mo	1.30	2.60	2.95	0.13	0.12	0.06	0.01	0.94	1.97	2.06	0.88	4.86	3.61	4.25	1.12
Nb	41.03	52.90	29.92	2.68	1.11	0.81	0.13	3.91	22.63	25.63	8.30	20.02	37.39	20.07	10.28
Ni	228.08	217.15	37.56	57.82	50.23	34.17	2.75	61.32	19.04	36.39	1173.32	56.11	52.39	58.15	277.92
Pb	33.28	36.24	22.69	36.94	1.12	24.74	0.77	330.80	27.27	15.63	2.29	17.45	25.16	17.62	13.73
Rb	911.93	972.15	113.76	805.21	1060.68	563.10	96.70	6486.11	234.66	56.81	5.12	76.12	150.91	76.26	15.43
Sc	66.61	74.54	42.58	24.07	18.47	14.84	1.49	26.22	36.28	35.74	38.30	39.13	48.41	40.60	42.16
Sr	419.97	535.27	1006.54	29.72	10.59	12.12	0.86	82.46	971.26	1050.18	136.01	757.02	1065.86	758.77	387.79
Ta	3.91	5.33	1.22	0.49	0.14	0.37	0.05	0.88	1.28	0.92	0.50	1.56	1.39	1.63	0.58
Th	25.30	34.24	1.54	1.48	0.28	0.57	0.03	27.58	9.11	1.26	1.15	21.36	2.52	21.32	2.46
U	6.52	9.03	1.15	40.67	40.20	0.57	40.20	39.97	2.52	1.16	0.19	9.29	1.52	9.24	0.56
V	438.21	425.66	215.76	158.11	151.37	80.66	6.86	151.11	261.19	204.93	330.00	309.58	262.45	313.25	263.14
W	2.13	1.92	0.64	27.15	24.63	13.62	1.07	140.01	3.58	0.31	0.11	1.72	0.91	1.42	0.38
Y	81.48	98.68	29.44	433.87	390.98	219.18	21.45	851.49	48.90	25.97	17.45	48.10	35.19	47.57	29.96
Zn	433.56	507.80	231.85	120.62	152.02	41.55	3.57	147.57	193.94	203.41	165.04	152.52	295.16	153.31	195.70
Zr	462.23	484.55	583.83	15.38	8.71	6.21	0.48	38.89	588.76	645.33	64.33	256.09	815.48	269.61	144.10
La	99.57	110.28	79.83	170.82	138.91	99.03	7.49	2024.48	57.66	100.31	15.27	61.82	101.17	61.91	42.01
Ce	198.55	218.62	156.26	17.42	12.72	9.52	0.69	192.88	118.15	198.27	42.27	136.15	200.53	137.29	88.04
Pr	22.25	24.19	17.55	60.15	43.11	32.11	2.19	603.06	14.31	21.62	5.62	16.08	22.53	15.93	9.75
Nd	89.40	92.57	71.17	9.39	5.74	4.83	0.34	73.32	60.98	82.78	24.79	64.41	89.93	62.69	38.46
Sm	17.87	19.64	11.70	1.96	2.26	1.23	0.11	8.39	12.03	13.25	4.96	12.43	14.77	12.15	7.51
Eu	3.64	2.79	3.92	7.30	4.12	3.36	0.25	39.80	3.29	3.91	1.38	3.32	4.61	3.17	1.52
Gd	14.89	18.48	9.18	0.93	0.43	0.44	0.03	4.02	10.55	10.00	4.90	10.77	10.86	10.19	6.92
Tb	2.28	3.08	1.14	5.88	2.35	2.60	0.17	18.89	1.49	1.17	0.65	1.40	1.39	1.38	0.97
Dy	14.79	17.71	6.18	1.03	0.39	0.43	0.03	2.70	9.34	5.64	3.94	9.07	7.47	8.59	5.82
Hf	12.26	13.38	13.71	1.04	0.26	0.27	0.02	4.71	12.75	15.99	1.85	6.82	19.20	7.39	3.81
Ho	2.95	3.50	1.14	2.83	0.92	1.16	0.08	6.72	1.85	0.99	0.70	1.70	1.36	1.72	1.11
Er	8.33	10.28	3.00	0.39	0.14	0.16	0.01	0.76	4.87	2.63	1.69	4.83	3.42	4.69	3.00
Tm	1.24	1.47	0.36	2.43	0.66	0.85	0.06	4.60	0.69	0.31	0.23	0.68	0.51	0.69	0.45
Yb	9.19	10.17	2.35	0.38	0.13	0.14	0.01	0.63	4.47	2.10	1.33	5.06	3.11	4.54	2.87
Lu	1.28	1.53	0.40	10.32	8.40	5.05	0.49	25.09	0.69	0.30	0.21	0.74	0.47	0.71	0.44
Σ REE	498.48	547.69	377.89	292.28	220.54	161.16	11.95	3010.05	313.12	459.27	109.79	335.27	481.33	333.01	212.67
(La/Yb)N	7.32	7.33	22.91	301.38	718.40	471.24	542.22	2158.93	8.71	32.34	7.76	8.26	21.99	9.22	9.89
(Gd/Yb)N	1.31	1.47	3.16	1.96	2.65	2.51	2.78	5.14	1.91	3.87	2.99	1.73	2.83	1.82	1.95
(Ce/Sm)N	2.14	1.36	1.86	1.53	5.55	2.68	2.69	3.22	2.37	3.61	2.05	2.64	3.24	2.73	2.83
Eu/Eu*	0.68	0.45	1.15	16.55	12.80	13.93	12.89	20.94	0.89	1.04	0.86	0.88	1.11	0.87	0.64

Table 4. Major (wt.%) and trace (ppm) element analyses ofrepresentative garnet and amphibole-rich gneiss, pyrigarnite and garnet-rich amphibolite from Eséka area

Rocks	Garnet and amphibole-rich gneiss				Pyrigarnite								Garnet-rich amphibolite					
Samples	ES1a	ES1b	ES1c	ES1d	ES2a	ES2b	ES2c	ES2d	ES2e	ES2f	ES2g	ES2h	ES3a	ES3b	ES3c	ES3d	ES3e	ES3f
wt.%																		
SiO2	63.4	60.5	63.2	60.3	48.5	48.65	46.88	47.36	48	47.9	50	53	48.2	47.88	48.75	48	47.5	45.76
TiO2	0.44	0.68	0.44	0.56	0.92	0.87	0.75	0.56	0.66	0.61	1.09	1.01	0.58	0.6	0.67	0.81	0.76	0.78
Al2O3	15.3	14.7	15.1	13.91	14.5	14.5	14.11	13.2	13.5	13.1	14.2	14.21	14.6	14.61	13.5	13.7	13.89	14.5
Fe2O3t	8.84	8.63	9.01	9.37	15.5	14.34	14.51	12.24	12.75	13.11	14.58	12.54	12.09	12.45	13.21	15.02	14.5	14.87
MnO	0.08	0.13	0.12	0.12	0.24	0.21	0.21	0.25	0.22	0.23	0.23	0.21	0.17	0.11	0.13	0.24	0.22	0.20
MgO	2.73	3.62	3.15	3.55	8.2	8.11	8.55	10.35	9.87	9.98	6.81	6.01	8.1	8.35	7.88	7.12	7.5	8.21
CaO	3.77	6.36	4.11	7.23	10.65	11.01	12.58	15.03	13.66	14.01	11.06	10.96	11.92	11.98	11.5	10.85	11.24	11.5
Na2O	3.08	3.33	3.18	3.21	2.12	1.88	1.97	1.2	1.35	1.35	1.88	2.01	2.75	2.11	2.34	2.12	2.55	2.41
K2O	2.22	1.7	1.88	2.02	0.09	0.07	0.04	0.04	0.05	0.05	0.45	0.51	1.47	1.55	1.61	1.72	1.65	1.66
P2O5	0.11	0.12	0.09	0.10	0.08	0.08	0.09	0.08	0.08	0.07	0.08	0.11	0.04	0.03	0.05	0.12	0.09	0.08
Total	99.97	99.65	100.19	100.27	100.8	99.72	99.69	100.30	100.14	100.41	100.29	100.46	99.93	99.67	99.64	99.70	99.90	99.97
ppm																		
Ba	795	519	789	657	27	21	25	23	21	25	128	141	375	398	401	562	455	543
Cr	46	90	51	98	78	123	150	693	487	550	145	135	198	212	197	202	189	191
Co	11	27	15	25	55	58	55	63	61	63	46	32	40	43	45	47	43	44
Cu	27	92	45	81	8	17	28	65	45	51	88	89	9	11	15	18	15	11
Ga	16	19	17	16	17	15	13	13	15	11	16	18	20	21	20	24	23	24
Nb	4	6	3	6	1	1	1	1	1	1	1	1	1	1	1	4	3	3
Ni	27	61	31	57	52	102	156	224	198	200	98	90	122	111	100	98	115	131
Pb	13	11	10	13	5	3	3	1	1	5	9	11	4	4	3	3	4	4
Rb	79	85	75	81	1	1	1	1	1	1	17	25	67	60	63	65	63	65
Sc	13	19	15	21	52	50	46	46	50	50	39	35	39	41	44	44	38	39
Sr	312	212	298	274	31	35	41	43	41	45	61	88	92	90	101	94	96	105
Ta	1.00	1.92	0.98	1.12	0.76	0.68	0.65	0.38	0.41	0.54	0.31	0.35	0.19	0.31	0.44	0.51	0.48	0.35
Th	7.19	7.23	6.98	7.01	0.22	0.33	0.35	0.40	0.31	0.31	0.20	0.23	0.25	0.31	1.23	1.96	1.51	1.66
U	0.51	0.75	0.55	0.65	0.08	0.06	0.08	0.08	0.06	0.08	0.10	0.41	0.94	0.87	0.73	0.65	0.66	0.71
V	66	163	87	174	359	331	344	245	288	301	318	228	230	245	251	267	255	258
Y	13	21	15	18	33	31	21	23	21	31	27	21	15	18	21	33	29	31
Zr	133	141	127	147	72	67	58	46	50	55	67	81	41	59	65	95	88	90
Zn	54	76	61	74	78	80	85	78	85	78	97	91	117	123	131	141	145	138
La	20.64	24.77	20.85	21.54	3.09	2.99	3.01	2.89	2.69	2.81	19.83	23.87	9.66	9.28	9.01	9.67	9.25	9.54
Ce	42.28	43.03	43.34	45.64	8.31	7.52	8.01	6.64	6.85	7.01	51.03	48.64	22.75	22.45	23.35	21.78	21.24	21.58
Pr	4.10	4.47	3.85	4.01	1.32	1.01	1.18	0.94	0.98	1.21	1.86	1.72	0.56	0.83	1.13	2.63	1.68	2.51
Nd	13.07	15.03	13.87	14.5	6.32	5.94	5.85	6.25	6.01	6.12	14.60	14.8	12.90	11.98	12.01	10.11	10.91	11.01
Sm	2.15	2.78	2.25	2.55	2.13	1.94	2.01	1.81	1.98	1.84	1.95	2.01	2.26	2.21	2.35	2.51	2.45	2.56
Eu	0.85	1.01	0.88	0.95	0.62	0.58	0.64	0.47	0.53	0.46	0.76	0.78	0.90	0.98	1.11	1.01	1.1	1.08
Gd	2.14	3.22	2.64	3.01	3.27	2.98	3.16	2.66	2.71	2.78	2.81	2.88	2.76	2.88	3.01	3.62	3.53	3.76
Tb	0.29	0.44	0.31	0.44	0.58	0.51	0.47	0.39	0.41	0.55	0.49	0.49	0.27	0.31	0.45	0.66	0.55	0.61
Dy	1.84	2.99	1.97	2.88	4.50	3.94	3.98	3.91	3.81	3.76	3.76	3.54	4.03	4.01	4.35	4.84	4.46	4.78
Hf	2.91	2.80	2.65	2.81	1.17	1.11	0.85	0.71	0.88	0.96	0.91	1.01	0.75	0.81	0.96	1.62	1.01	1.44
Ho	0.32	0.52	0.45	0.51	0.90	0.88	0.75	0.61	0.68	0.74	0.74	0.63	0.38	0.44	0.65	0.97	0.91	0.88
Er	0.94	1.57	0.98	1.48	2.80	2.56	2.6	2.68	2.51	2.41	2.18	2.02	2.50	2.45	2.65	2.96	2.91	2.95
Tm	0.15	0.23	0.21	0.18	0.41	0.4	0.38	0.29	0.31	0.35	0.32	0.3	0.18	0.23	0.35	0.46	0.41	0.45
Yb	0.90	1.56	0.96	1.52	2.70	2.4	2.2	2.61	2.21	2.18	2.12	1.98	2.66	2.68	2.72	2.86	2.66	2.88
Lu	0.14	0.23	0.16	0.21	0.43	0.41	0.36	0.42	0.38	0.4	0.32	0.3	0.39	0.4	0.35	0.43	0.38	0.41
Σ REE	92.73	104.64	95.37	102.23	38.55	35.17	35.45	33.27	32.94	33.58	103.68	104.97	62.95	61.94	64.45	66.13	63.52	66.44
(La/Yb)N	15.45	10.73	14.68	9.58	0.77	0.84	0.92	0.75	0.82	0.87	6.32	8.15	2.45	2.34	2.24	2.28	2.35	2.24
(Gd/Yb)N	1.92	1.67	2.23	1.60	0.98	1.01	1.16	0.83	0.99	1.03	1.07	1.18	0.84	0.87	0.90	1.02	1.08	1.06
(Ce/Sm)N	4.74	3.74	4.65	4.32	0.94	0.94	0.96	0.89	0.84	0.92	6.33	5.84	2.43	2.45	2.40	2.09	2.09	2.03
Eu/Eu*	1.21	1.03	1.10	1.05	0.72	0.74	0.78	0.65	0.70	0.62	0.99	0.99	1.10	1.19	1.28	1.02	1.14	1.06

4. Results

4.1. Rock Lithology

The Edéa and Eséka areas are made up of three distinguish rock units. The first unit is of sedimentary parentage, the second of clear igneous origin and the third from the melting. All these three units contain quartzo-feldspathic segregations arising from either in situ partial melting or injection along dykes or ductile shear zones. However detail observations and sampling were essentially carried out by mapping. Mineral abbreviations are given by Kretz [16].

4.1.1. The Metasedimentary Unit

This unit is composed of garnet-rich micaschist and schist. Garnet-rich micaschist are the most important types

and outcrop as flagstones (Figure 3 a). They are fine to medium-grained with alternating millimetre quartzo-feldspathic and ferromagnesian layers. Granoblastic microstructures prevail in this rock type but flaser and mylonitic ones are frequently observed. Garnet-micaschist are composed of biotite (8-10%), muscovite (10-20%), garnet porphyroblasts (15-20%), quartz (25-30%), plagioclase (20-25%), accessories mineral are monazite and oxide (Figure 3 b).

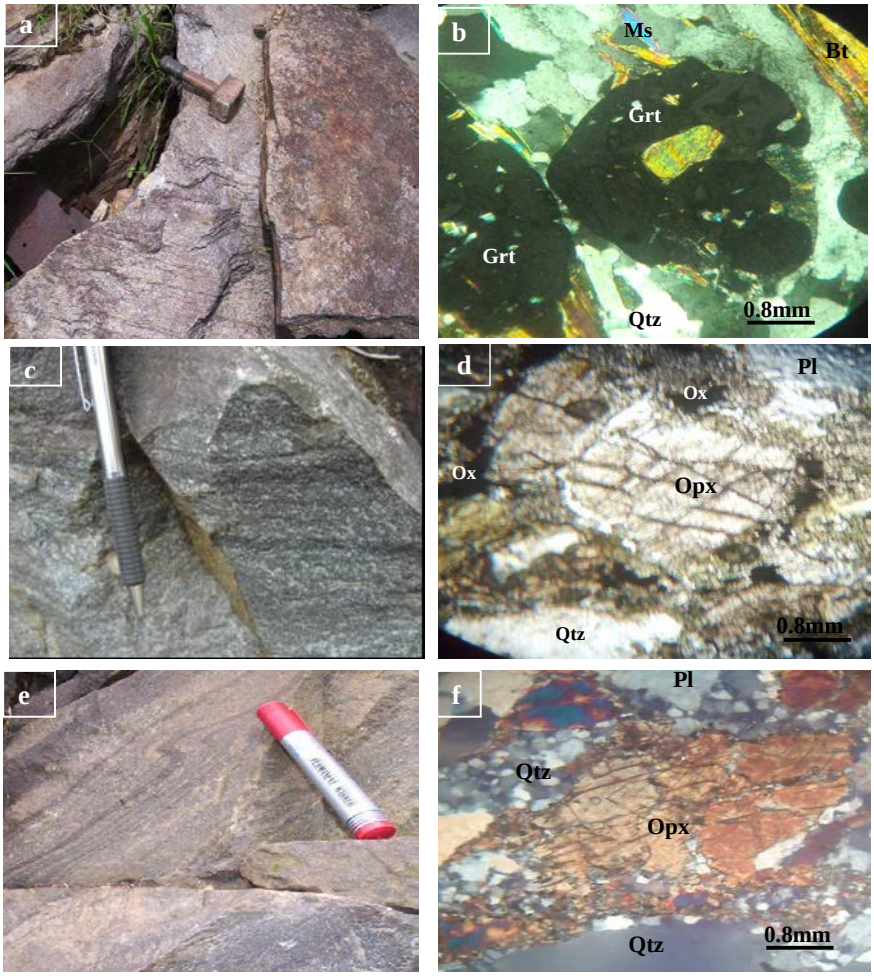

Figure 3. (a) Flat outcrop of garnet bearing micaschist; **(b)** Photomicrograph of garnet-bearing micaschist displaying garnet porphyroblast containing biotite and muscovite as inclusions. **(c)**Detail outcrop view of pyroxene-rich gneiss. Note thethin alternation of ferromagnesian and quartzo-feldspathic layers. **(d)**Photomicrograph of pyroxene-rich gneiss showing almond-shaped orthopyroxene crystal displaying a rim composed of Qtz + Pl + Ox. **(e)**Outcrop view of garnet-rich charnockitic gneiss; **(f)**Orthopyroxenemegacrystal displaying corona of Qtz + Pl in garnet-bearing charnockitic gneiss; (Qtz: quartz; Pl: plagioclase;Grt: garnet; Opx: orthopyroxene; Ms: muscovite; Bt: biotite; Ox: opaque oxide)

4.1.2. The Meta-Igneous Unit

The meta-igneous rocks consist of pyroxene-rich gneiss, charnockitic-rich gneiss, pyribolite, amphibolite, amphibole and biotite-rich gneiss, biotite-rich gneiss, garnet-amphibole-rich gneiss, garnet-rich amphibolite and pyrigarnite. Granoblastic microstructures prevail in all rock types, although flaser and mylonitic ones are also commonly observed.

Pyroxene-gneiss (Figure 3 c) occurs as dome and block. They are fine to medium-grained, dark-gray colored rocks displaying alternating millimetre to decimetre ferromagnesian and quartzo-feldspathic layers. They display granoblastic and corona microstructures and composed of quartz (28-30%), plagioclase (15-18%), almond-shaped orthopyroxene (20-22%) showing corona composed essentially of Qtz + Pl and Qtz + Pl + Ox (Figure 3 d); hornblende (< 9%), biotite (15-17%), ovoid and kelyphitic garnet (11-13%) crystals displaying symplectitic association of Hbl + Bt + Qtz + Pl. Accessories mineral are oxides.

Garnet-charnokitic gneiss (Figure 3 e) are medium-grained and outcrop as dome. They display coloured minerals (quartz and feldspath are blue-yellowish in colour). The microstructures are granoblastic although rims are observed on some minerals. These rocks consist of quartz (37-40%), plagioclase (< 7%), almond-shaped orthopyroxene crystals (18-20%) displaying corona of Qtz + Pl + Px ± Bt, biotite (13-15%) (Figure 3 f), garnet porphyroblasts (23-25%) surrounded by Qtz + Pl + Bt-rich rim. Monazite and oxides are accessories minerals.

Garnet and amphibole-rich gneiss outcrop as flagstone and blocks; they are composed of hornblende (15-18%) partly replacing pyroxene and displaying transformation in quartz and biotite, quartz (20-22%), plagioclase An_{26-31}, (20-21%), K-feldspar (< 5%), orthopyroxene (< 10%), garnet (10-12%), biotite (18%). Accessories are zircon and apatite.

Pyrigarnite occurs as blocks and as boudins, they display granoblastic and corona microstructures. They are made up of quartz (17-20%), plagioclase An_{26-31} (13-15%), K-feldspar (< 10%), orthopyroxene (27-30%) with rim of

Qtz + Pl; hornblende (< 5%), garnet porphyroblasts (22-25%) with rims of Qtz + Kfs, Pl + Px, Pl + Qtz. Accessories are apatite, rutile and oxides.

Garnet-rich amphibolite occurs as blocks, boudins and flagstone and display granoblastic and corona microstructure. They composed of quartz (17-20%), amphibole (27-30%) partly replacing pyroxene; kelyphitic garnet (22-25%) displaying Pl + Qtz-rich rim and symplectitic association of Hbl + Px; pyroxene (< 12%), plagioclase An_{24-26} (12-15%). Accessories are apatite, zircon and oxides.

4.1.3. The Migmatites and TTG

Rocks resulting from the melting are composed of migmatites and TTG (tonalites, trondhjemites and granodiorites) suit. Migmatites are the most dominant type and occur as flagstones. They composed of quartz (27-30%), plagioclase (25-30%), perthitic K-feldspar (7-10%), amphibole (<10%) displaying transformation of biotite; garnet (< 10%) showing Pl + Qtz-rich rim; biotite (5-10%), pyroxene (12-15%). Accessories are zircon and oxides. TTG rocks are well known in the Congo Craton (e.g. [1,2,3,6,17,18,19,20,21]).

4.2. Whole-Rock Chemistry and Nature of the Protoliths

Chemical composition of the studied rocks is presented in Table 1 to Table 4. We used the $Fe_2O_3t + TiO_2 + CaO$ vs. Al_2O_3 whole rocks diagram of De la Roche [22] to determine the protolith of the different petrographic type. In this diagram, meta-igneous define a chemical trend parallel to the igneous rocks origin, while metasediments plot in the shale field (Figure 4). These metashale are similar to other shale documented in the literature (e.g. [23-30]).

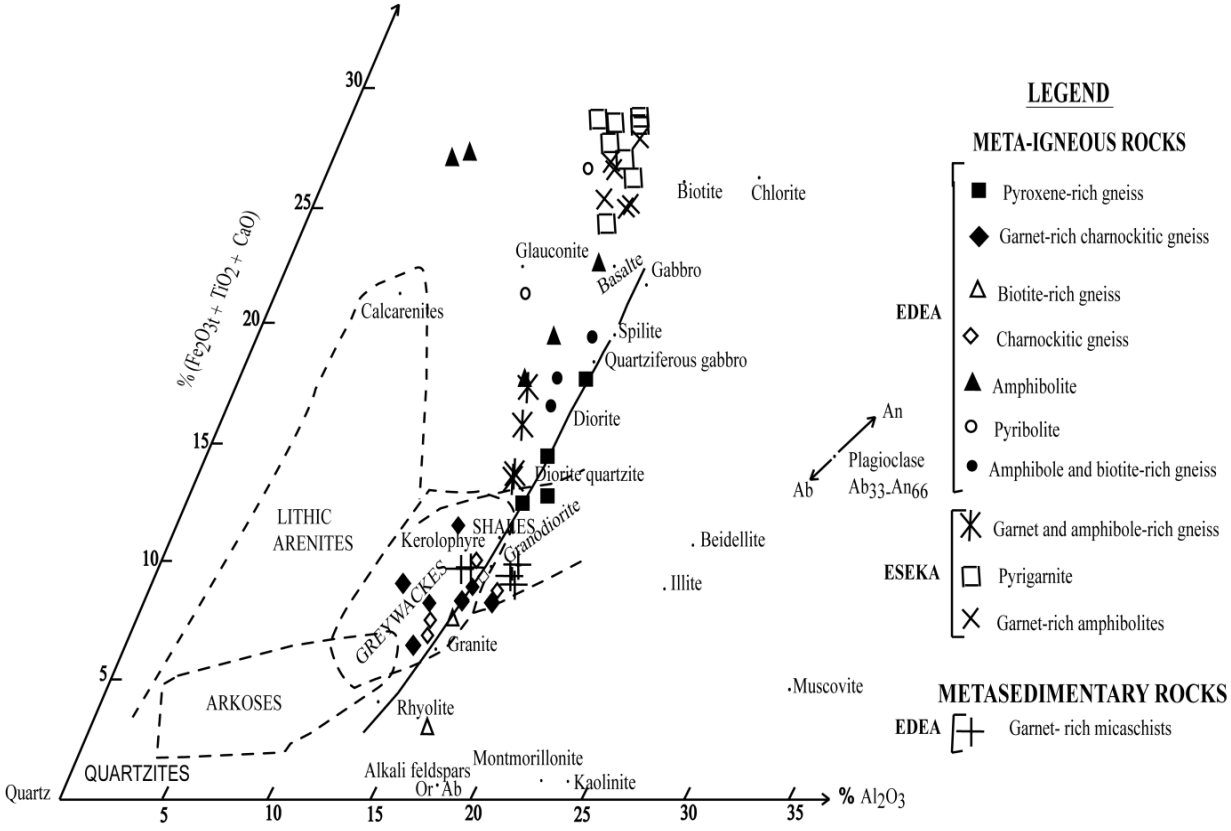

Figure 4. $Fe_2O_3t + TiO_2 + CaO$ vs. Al_2O_3 diagram of De la Roche [22] showing the whole rock chemical composition of the studied rocks

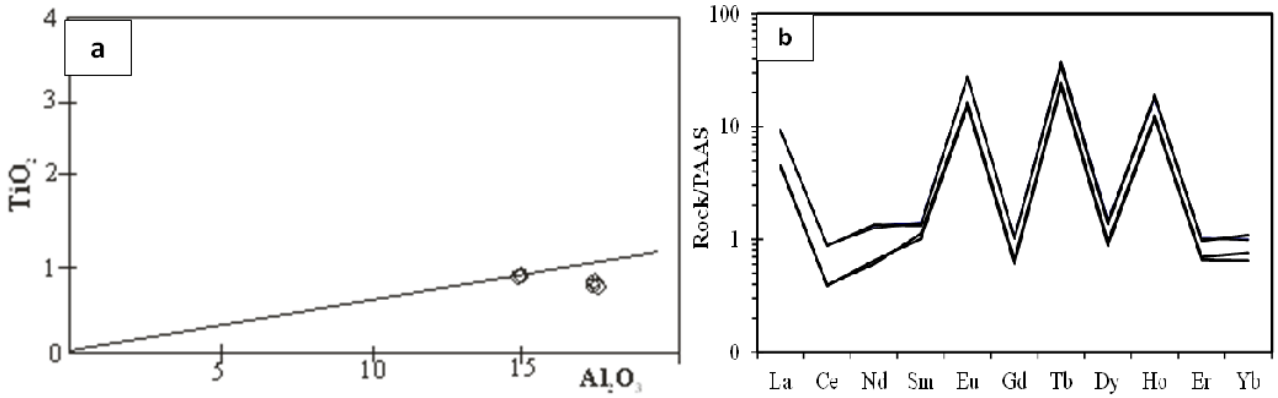

Figure 5. Distinctive variationdiagrams for the metasedimentary unit. (a) Pot of TiO_2 vs. Al_2O_3, the solid line corresponds to the TiO_2/Al_2O_3 ratio for clay afterGoldschmidt [31]; (b) PAAS normalised-REE patterns

4.2.1. Metasedimentary rocks

Garnet-rich micaschist display all the features of pelitic rocks with FeO, MgO, K_2O and TiO_2 closely correlated to Al_2O_3 (Table 1; Figure 5 a). All these elements are anticorrelated with silica suggesting that these gneisses were composed of a quartz-clay mixture. Their average composition corresponds closely to those of Post-Archean shale [25]. Their TiO_2 content (0.76-0.82%) and average TiO_2/Al_2O_3 (0.04) ratio are similar to those of clay (0.040 according to Goldschmidt, [31] 1954; 0.03-0.05 according to Taylor and McLennan, [25], similar to average terrigeneous and correspond to values given for continental or near-shore argillaceous and arenaceous sediments [32]. The overall chemical patterns are closed to the Neoproterozoic metashales of Yaoundé [7,33,34] and Paleoproterozoic metashales of Banyo [26]; Kekem [35], and Bossangoa-Bossembele in Central African Republic [29]. Trace element contents are high suggesting that these rocks are distinct from passive and active margin greywackes [36], but have some similarities with alkaline rocks. The average Nb/Y ratio (0,004) and the fractionated REE (601-1170 ppm) elements suggest that these metasediments could be derived from reworking of alkaline volcanic rocks. Their REE patterns are fractionated, with a high positive Eu anomaly (Figure 5 b).

4.2.2. Meta-igneous rocks

According to the silica contents, pyroxene-rich gneiss are intermediate rocks (55 < SiO_2 <61.3%). These chemical compositions are those of quartz-diorite (Figure 6). They are rich in Al_2O_3, Fe_2O_3, MgO, Na_2O, Na_2O + K_2O, Ba, Rb but poor in K_2O, CaO, Sr (Table 2). TiO_2 contents and FeO^*/MgO ratios varies from 0.35 to 0.76% and 1.35 to 3 respectively. The iron enrichment with the values of titanium in these rocks is comparable to those of the tholeiitic series. Also, CaO/TiO_2 (3.19-10) and Al_2O_3/TiO_2 (22-47.86) ratios correspond closely to those of oceanic tholeiite [37,38]. However Y/Nb (2.15-241.35) ratios > 1 are similar to those of tholeiite ([39] Pearce and Cann, 1973). Plotting in the TiO_2 vs. FeO*/MgO diagram [40] (Figure 6), pyroxene-bearing gneiss fall in the tholeiites field. Their REE patterns (Figure 7 a) are very strongly fractionated (La_N/Yb_N = 6.67-353.47); LREE enriched (Ce_N/Sm_N = 0.81-2.15), HREE enriched (Gd/Yb_N = 1.56-2.36) and displays a high positive Eu anomaly (Eu/Eu* = 0.88-17.61). All these features are due to the accumulation of pyroxenes. Their overall trace element patterns (Figure 7 b) show Ba, Th, Nb, Sr, Zr, Yb anomaly, indicating after Thompson et al. [42] their crustal and mantle origin.

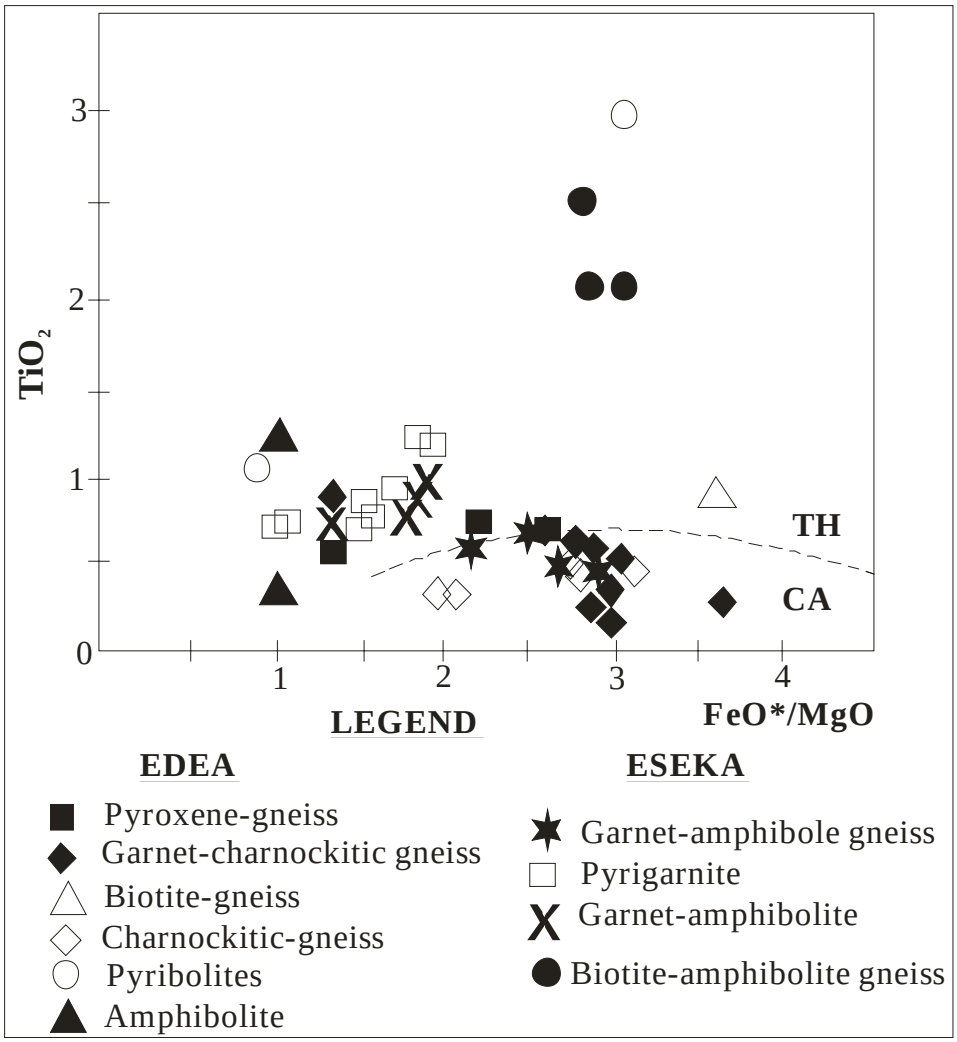

Figure 6. TiO_2 vs. FeO*/MgO diagram of Miyashiro [40] showing calc-alkaline and tholeiitic characters of meta-igneous rocks from Edéa and Eséka areas

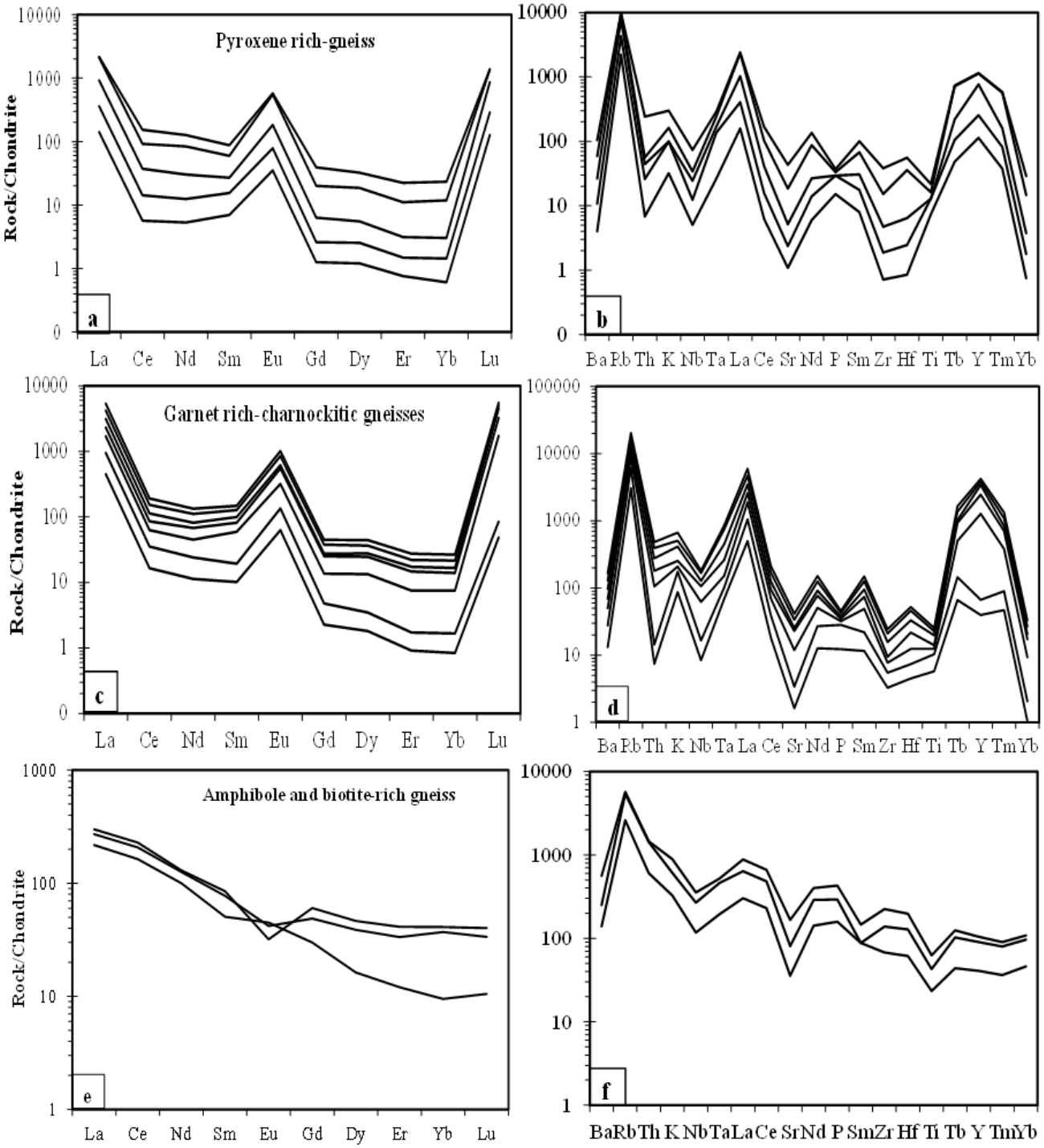

Figure 7. Chemical patterns for meta-igneous rocks from Edéa area. (a, c, e) Chondrite-normalised REE patterns.Normalized values after Evensen et al. [41]; (b, d, f) Chondrite-normalised trace element patterns. Normalised values after Thompson et al. [42]

Garnet-bearing charnokitic gneiss are slightly scattered in composition (Table 2). These rocks are silica-rich with a total range of SiO_2 between 66.23 to 72%; these chemical compositions are those of granite (Figure 4). They display distinctly higher CaO, Na_2O, Ba, Sr, REE and low TiO_2, MgO, K_2O contents and the total alkali concentrations varies from 3.32-5.65%. Ba/Sr, Ba/Rb and K/Rb ratios are similar to those observed in continental calc-alkaline igneous suites [43-61]. These rocks display the characteristics of calc-alkaline series (Figure 6). Their REE patterns (Figure 7 c) are very strongly fractionated (La_N/Yb_N = 96.8-598) and resemble those of pyroxene-gneisses; LREE enriched (Ce_N/Sm_N = 0.7-2), HREE enriched (Gd/Yb_N = 0.9-3) and display a high positive Eu anomaly (Eu/Eu* = 9.8-15). Their overall trace element patterns (Figure 7 d) show Ba, Th, Nb, Sr, P, Zr, Ti, Yb anomalies, indicating after Thompson et al. [42] their crustal and mantle origin.

Amphibole and biotite-rich gneiss have the composition of gabbro and quartz-diorite rocks (Figure 4). They are deficient in silica (49.13 to 53.36%) and rich in K_2O (≈ 4%). They also have high FeO and MgO contents and exceptionally high P_2O_5 and REE contents (Table 3). The Figure 6 shows that these rocks have tholeiitic affinity. The REE patterns (Figure 7 e) are strongly fractionated (La_N/Yb_N = 7.32-23) with high LREE enrichment (Ce_N/Sm_N = 1.36-2.41), HREE depletion and negative Eu anomaly (Eu/Eu* = 0.44-1.15). Trace element distribution

patterns display Ba, Th, Nb, Sr, Sm, Ti, Tm anomalies (Figure 7 f). All these chemical features are similar to those of ultramafic and mafic varieties of alkaline rocks [7,62,63,64,65,66]. Garnet-bearing amphibolite and pyrigarnite have the composition of gabbroic rocks (Figure 6) with a silicate content ranging from 46 to 49% and from 47 to 53% respectively (Table 4). The higher FeO and MgO contents together with high Cr and Ni contents and with constant Y and Nb contents suggest that their more mafic composition is related to accumulation of pyroxene rather than to a less differentiated nature. TiO_2 (0.56-1.09%) contents varies with FeO (12-15.5%) contents, these variations are similar to those of magmatic tholeiitic series. The REE pattern (Figure 8 a & Figure 8 b) are sub-flat and fractionated (La_N/Yb_N = 0.75-8.15) with à LREE enrichment of 10 to 100 times chondritic values (Ce_N/Sm_N = 0.83-6.33), and a weak negative Eu anomaly (Eu/Eu* = 0.61-1.2). This suggests that they could be of transitional or alkaline affinity [52]. Trace element distribution patterns of garnet-bearing amphibolites display Ba, Th, Nb, Sr, Ti, Tm (Figures 8c & 8d), indicating after Thompson et al. [42] their crustal and mantle origin; and Rb, Nb, La, Sr, Sm, Ti for pyrigarnites anomalies (Figure 8 d), indicating their crustal origin [42].

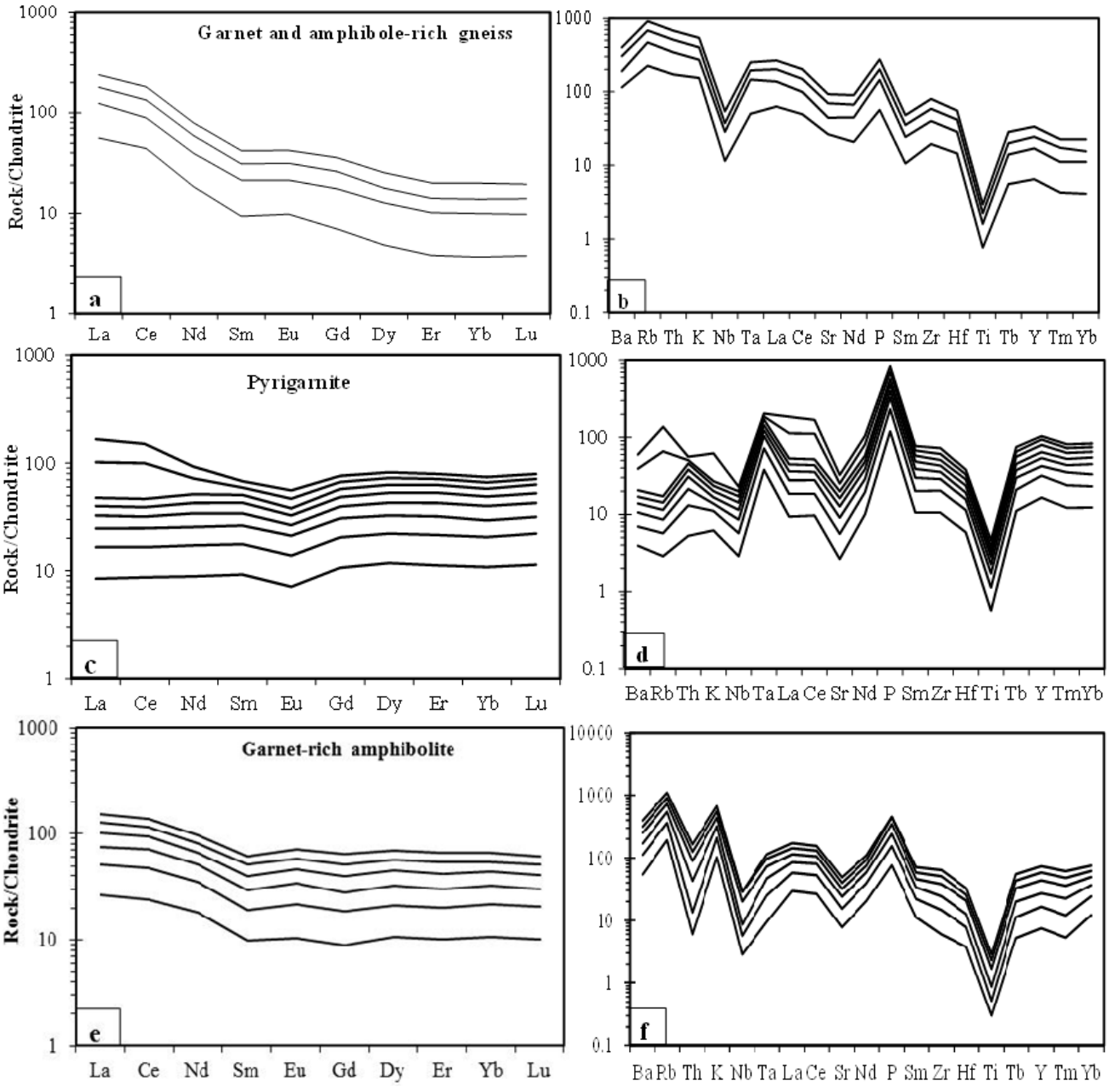

Figure 8. Chemical patterns for meta-igneous rocks from Eséka area. (a, c, e) Chondrite-normalised REE patterns.Normalized values after Evensen et al. [41]; (b, d, f) Chondrite-normalised trace element patterns. Normalised values after Thompson et al. [42]

5. Discussion

The main lithology of Edéa and Eséka area corresponds to (1) a metasedimentary unit rocks make up of garnet-bearing micaschist and schist with chemical patterns have similarity with Neoproterozoic and Paleoproterozoic metashale. Schist are well known in the neighboring series: Yaoundé series [7,67], Mbalmayo-Bengbis- Ayos series [7,67,68]; (2) a meta-igneous unit rocks comprise pyroxene-rich gneiss, garnet-rich charnockitic gneiss, charnockitic gneiss, amphibole and biotite-rich gneiss, biotite-rich gneiss, pyribolite, amphibolite, garnet and amphibole-rich gneiss, garnet-rich amphibolite and

pyrigarnite; these rocks display chemical patterns similar to those of the Pan-African and Paleoproterozoic rocks in central Cameroon regions such as the Maham III [60] and Banyo mafic meta-igneous rocks [26,66]. All the major and trace element patterns of metasediments have the composition of shale and similar to Post-Archean shale [25] and close to those of continental or near-shore argillaceous sediments. The average Nb/Y (0.004) ratio and the fractioned REE patterns suggest that the contribution of alkaline vulcanite and a continental environment can be envisaged for these metasediments.

Metasedimentary rocks extend to the Yaoundé series [7,30,69] and Ayos-Mbalmayo-Bengbis series [7,68] which is largely dominated by the Neoproterozoic metasedimentary sequence; the protoliths of these series were deposited in a passive margin environment at the northern edge of the Congo Craton. The lithological assemblage constituting the Yaoundé series clearly corresponds to a depositional environment related to an emerged continent and thus a derivation of the sediments from the Congo Craton seems likely.

The investigated Edéa and Eséka meta-igneous rocks exhibit petrographical and chemical compositions characteristic of intermediate to basic tholeiitic and calc-alkaline rocks [40] derived from igneous protoliths varying from granites to gabbros. The calc-alkaline rocks display high FeO*/MgO (1.5-3.31) ratios. The tholeiitic rocks are characterised by high TiO_2 (0.6-3.47%) contents and their chemical compositions correspond to those of continental tholeiite [25,70,71,72], with Th/Ta ratios and Nb relatively high (Table 2, Table 3 and Table 4), characterizing the tholeiites linked to rifting [73,74,75,76,77]. The calc-alkaline affinity characterizes the compressive orogenic domain while the tholeiitic affinity characterizes the distensive orogenic domain. This double affinity of the source (calc-alkaline/tholeiite) indicates a double paleoenvironment: calc-alkaline affinity indicates thickening environment while tholeiitic affinity characterizes extensive environment. This result is similar to those obtained in the central domain of the Pan-African fold belt, where Pan-African calc-alkaline rocks (biotite-amphibole gneiss, orthogneiss, S-C mylonitic granites, leucogranites) and Paleoproterozoic tholeiitic rocks (garnet-amphibole gneisses, banded amphibolites, garnet-amphibolites) are recorded in Tonga region [78].

The nature of the igneous source can be constrained using the geochemical signatures of the meta-igneous rocks. The REE and multi-elements patterns (Figure 7 and Figure 8) suggest genetic processes involving both participation of the crust and the mantle [42]. The recent work of Tanko Njiosseu [78] also recorded crustal and mantle origin for the meta-igneous rocks of Tonga located in the central domain. This allows us to conclude that, the Nyong series and central domain of Pan-African fold belt represent an ancient continental domain which has been reworked. The rocks of these domains have been affected by thrusting, and this thrust continues towards the East, forming the Oubanguides Nappe in the Republic of Central Africa and towards the NE Brazil in the Borborema province.

The high contents of LREE (10 to 100 times Chondrite values) in these rocks could be related either to the enrichment of their source materials in LREE or to the presence of mineralization fluids. Moreover the spider diagrams characteristically display negative anomalies for Ba, Th, Nb, Sr, P, Zr, Ti, Yb. These anomalies result either from the low content of these elements in the source, or their retention in the residue during partial melting.

6. Conclusions

1. The Nyong series comprises a metasedimentary unit rocks make up of garnet-bearing micaschist and schist, and main meta-igneous unit rocks (pyroxene-rich gneiss, garnet-rich charnockitic gneiss, charnockitic gneiss, amphibole-biotite-rich gneiss, biotite-rich gneiss, pyribolite, amphibolite, garnet-amphibole-rich gneiss, garnet-rich amphibolite and pyrigarnite).

2. Metasediments have the composition of shale and close to those of continental or near-shore argillaceous sediments. Meta-igneous rocks exhibit the compositions of intermediate to basic tholeiitic and calc-alkaline rocks derived from continental igneous protoliths varying from granites to gabbros.

3. The Study area has experienced the compressive and the tholeiitic orogenic domain indicatives of a duality paleo-environment: thickening environment and distensive environment.

4. The REE and multi-elements patterns are in accordance with genetic processes involving both participation of the crust and the mantle.

5. The recent work in Central domain of the Panafrican North Equatorial Fold Belt [26,56,78] which also documented crustal and mantle origin for the meta-igneous rocks allows us to conclude that, the western border of the Congo craton and central domain of the fold belt represent an ancient continental domain which has been reworked during the later events (Pan-African orogeny for the central domain and probably Paleoproterozoic orogeny for the Nyong series). The rocks of these domains were thrust towards the South and towards the East, forming the Oubanguides Nappe in the Republic of Central Africa and towards the NE Brazil in the Borborema province.

Acknowledgements

The data presented here form a part of the first author's Ph. D thesis supervised by J.P. Nzenti and E. Suh Cheo. Thanks are due to We gratefully acknowledge the Institute of Mineralogy and Geochemistry of the University of Lausanne (Switzerland) for providing facilities for whole rock geochemical analyses. Thanks are due to Dr Ganno Sylvestre (University of Yaoundé 1) for the comments and suggestions of earlier version of the manuscript.

References

[1] Pouclet, A., Tcahameni, R., Mezger, K., Vidal, M., Nsifa, E.N., Shang, C. and Penaye J. Archaean crustal accretion at the Northern border of Congo Craton (South Cameroon):The charnockite-TTG ling. *Bulletin Société Géologique France*, 178, 331-342, 2007

[2] Toteu, S.F., Penaye, J., Van Schmus, W.R., and Michard A. Preliminary U/Pb and Sm/Nd geochronologic data on the North-Central Cameroon: contribution of an Archaean and Paleoproterozoic crust to the edification of an active domain of the

Pan-African orogeny. *Comptes Rendus de l'Académie des Sciences Paris*, 319, 1519-1524,1994

[3] Shang, C.K., Liégeois, J.P., Satirb, M., Frisch, W. and Nsifa, E.N. Late Archaean high-K granite geochronology of the northern metacratonic margin of the Archaean Congo Craton, Southern Cameroon: Evidence for Pb-loss due to non-metamorphic causes *Gondwana Research*, 18 (2-3), 337-355, 2010.

[4] Goodwin, A.M. Precambrian geology — the dynamic evolution of the continental crust. *Academic Press. Harcourt Brace Jovanovich Publishers*, 666 pp, 1991.

[5] Maurizot, P., Abessolo, A, Feybesse, J.L., Johan V. and Lecomte P. Etude et prospection minière du Sud-Ouest Cameroun. Synthèse des travaux de 1978 à 1985. *Rapport BRGM*, Orléans 85, CMR 066, 274 pp, 1986.

[6] Nedelec, A., Nsifa, N.E. and Martin, H. Major ant trace element geochemistry of the Archaean Ntem plutonic complex (South Cameroon): petrogenesis and crustal evolution. *Precambrian Research*, 47, 35-50, 1990.

[7] Nzenti, J.P., Barbey, P., Macaudiere, J. and Soba, D. Origin and evolution of the late Precambrian high-grade Yaounde gneisses (Cameroon). *Precambrian Research*, 38, 91-109, 1988.

[8] Barbey, P., Macaudière, J., Nzenti, J. P. High pressure dehydration melting of metapelites: evidence from migmatites of Yaounde (Cameroon). *Journal of Petrology* 31, 401-427, 1990.

[9] Mvondo, H., Den Brok, S. W.J. and Mvondo Ondoa, J. Evidence for extension and exhumation of the Yaounde nappe (Pan-African fold belt, Cameroon). *Journal of African Earth Sciences* 36, 215-231, 2003.

[10] Toteu, S.F., Penaye, J., Deloule, E., Van Schmus, W.R. and Tchameni, R.. Diachronous evolution of volcano-sedimentary basins north of the Congo Craton: insights from U/Pb ion microprobe dating of zircons from the Poli, Lom and Yaoundé Groups (Cameroon). *Journal of African Earth Sciences* 44, 428-442, 2006.

[11] Delhal, J. and Ledent, D. Musée Royal Afrique Centrale. *Tervuren. Rapp. Ann.* 1974, pp. 71-76, 1975.

[12] Lasserre, M., Soba, D. Age Libérien des granodiorites et des gneiss à pyroxènes du Cameroun Méridional. *Bulletin BRGM 2* (4), 17-32, 1976.

[13] Tchameni, R., Pouclet, A., Mezger, K., Nsifa, N.E. and Vicat, J.P. Monozircon and Sm-Nd whole rock ages from the Ebolowa greenstone belts: Evidence for the terranes older than 2.9Ga in the Ntem Complex (Congo craton, South Cameroon). *Journal of Cameroon Academic of Sciences*, 4, 213-224, 2004.

[14] Toteu, S.F., Van Schmus, W.R., Penaye, J., Michard, A. New U-Pb and Sm-Nd data from north-central Cameroon and its bearing on the pre-PanAfrican history of Central Africa. *Precambrian Research*, 108, 45-73, 2001.

[15] Lerouge, C., Cocherie, A., Toteu, S.F., Penaye, J., Milesi, J.P., Tchameni, R., Nsifa, N.E., Fanning, C.M. and Deloule, E. SHRIMP U/Pb zircon age evidence for paleoproterozoic sedimentation and 2.05 Ga syntectonic plutonism in the Nyong Group, South-western Cameroon: consequences for the eburnean-transamazonian belt of NE Brasil and central Africa. *Journal of African Earth Sciences*, 44, 413-427, 2006.

[16] Kretz R. Symbols for rock-forming minerals. *American mineralogist*, 68, 277-279, 1983.

[17] Feybesse, J.L., Johan, V., Maurizot, P. and Abessolo, A. Evolution tectono métamorphique libérienne et éburnéenne de la partie NW du Craton Zaïrois (SW Cameroun). *In G. Matheis and H. Schandelmeier (Editors), Current research in African Earth Sciences. Balkema, Rotterdam*, 9-12, 1987.

[18] Shang, C.K., Satirb, M., Siebel, W., Taubald, H., Nsifa, E.N., Westphal, M. and Reitter E. Genesis of K-rich granitoids in the Sangmelima region, Ntem complex (Congo craton), Cameroon. *Terra Nostra*,5, 60-63, 2001.

[19] Shang, C.K., Satirb, M. Siebelb, W. Nsifa, N.E. Taubald, H., Liegeois, J.P. and Tchoua F.M. TTG magmatism in the Congo craton; a view from major and trace element geochemistry, Rb-Sr and Sm-Nd systematics: case of the Sangmelima region, Ntem complex, Southern Cameroon. *Journal of African Earth Sciences*, 40, 61-79, 2004 a.

[20] Shang, C.K., Siebel, W., Satirb, M., Chen, F. and Mvondo, O.J. Zircon Pb-Pb and U-Pb systematics of TTG rocks in the Congo craton: constraints of crustal formation, crystallization and Pan-African lead loss. *Bulletin of Geosciences*, 79, 205-219, 2004 b.

[21] Shang, C.K., Satirb, M., Nsifa, E.N., Liegeois, J.P., Siebel, W., Taubald, H. Archaean high-K granitoids produced by remelting of the earlier Tonalite-Trondhjemite-Granodiorite (TTG) in the Sangmelima region of the Ntem complex of the Congo craton, southern Cameroon. *International Journal of Earth Sciences*, 96, 817-842, 2007.

[22] De la Roche, H. Sur l'existence de plusieurs faciès géochimiques dans les schistes paléozoïques des Pyrénées lychonnaises. *Geol. Rundsch.*, 55, 274-301, 1965.

[23] Nance, W.B. and Taylor, S.R. Rare earth element patterns and crustal evolution I. Australian post-Archean sedimentary rocks. GCA, 40, 1539, 1976.

[24] McLennan, S.M. Trace element geochemistry of sedimentary rocks: implications for the composition and Evolution of the continental crust. *Ph.D. Thesis, Australian National University*. 1981.

[25] Taylor, S.R. and Mc Lennan, S.M. The continental crust: its composition and evolution. An examination of the geochemical record preserved in sedimentary rocks. *Blackwell Science Publications*, 312p, 1985.

[26] Nzenti, J.P., Tanko Njiosseu, E.L. and Nzina N.A. The metamorphic evolution of the Paleoproterozoic high grade Banyo gneisses (Adamawa, Cameroon, Central Africa). *Journal of African of Cameroon Academy of Sciences*, 7 (2), 95-109, 2007.

[27] Tchaptchet, T.D., Nzenti, J.P, Njiosseu, E.L., Ngnotué, T. and Ganno, S. Neoproterozoic metamorphic events in the kekem area (Central domain of the Cameroon North Equatorial Fold Belt): P-T data. *Journal of the Cameroon Academy of Sciences*, 8, N°2/3, 91-105, 2009a.

[28] Tchaptchet, T.D., Schulz, B. and Nzenti, J.P. Electron microprobe dating and thermobarometry of Neoproterozoic metamorphic events in the Kekem area, Central African Fold Belt of Cameroon. *Nueue Jahbur für Mineralogy Abh.*, 186/1, 95-109, 2009 b.

[29] Danguene, P.E.L. Géologie de la région de Bossamgoa-Bossembélé au Nord-Ouest de la République Centrafricaine (chaîne panafricaine Nord Equatorial): Pétrogenèse, structurogenèse et géochronologie. *Unpublished Ph.D Thesis, Université de Yaoundé I*, 121 p, 2012.

[30] Ngnotué, T., Ganno, S., Nzenti, J.P., Schulz, B., Tchaptchet Tchato, D. and Suh Cheo, E. Geochemistry and geochronology of Peraluminous High-K granitic leucosomes of Yaoundé series (Cameroon): evidence for a unique Pan-African magmatism and melting event in North Equatorial Fold Belt. *International Journal of Geosciences*, 3, 525-548, 2012.

[31] Goldschimidt, H. J. Geochemistry, *Clarendon Press*, 1954.

[32] Migdisov, A. A. On the titanium-aluminium ratio in sedimentary rocks. *Geochim. U.S.S.R.*, 2, 178-194, 1960.

[33] Nzenti J. P., Barbey P., Tchoua F.M. Evolution crustale au Cameroun: éléments pour un modèle géodynamique de l'orogenèse néoproterozoïque. *In* Géologie et environnements au Cameroun, Vicat et Bilong editors, *collection GEOCAM 2*, 397-407, 1999.

[34] Ngnotué T., Nzenti J. P., Barbey P. and Tchoua, F. M. The Ntui-Betamba high-grade gneisses: a Northward extension of the Pan-African Yaounde gneisses in Cameroon. *Journal of African Earth Sciences*, 31, 369-381, 2000.

[35] Tchaptchet, T.D. Geology of the Kekem area (Cameroon central domain): Metamorphic Petrology, P-T-t path, EMP, LA-ICPMS dating and implications for the geodynamic evolution of the Pan-African North Equatorial fold belt. Unpublished Ph. D thesis, University of Yaoundé 1, 110 pp, 2011.

[36] Bhatia, M.R. and Crook, A.W. Trace element characteristics of greywackes and tectonic setting discrimination of sedimentary basins. *Contribution to Mineralogy and Petrology*, 92, 181-193, 1986.

[37] Shibata,T., Thompson, G. and Frey, F.A. Tholeiitic and alkali basalts from the middle Atlantic ridge at 43°N. *Contribution to Mineralogy and Petrology*, 70, 127-142, 1979.

[38] Leeman, W.P., Budahan, J.P., Gerlach, D.C., Smith, D.R. and Powell, B.N. Origin of Hawaiian tholeiites : trace element contraints. American Journal of Science, 280 A, 794-819, 1980.

[39] Pearce, J.A. and Cann, J.R. Tectonic setting of basic volcanic rocks determined using trace element analyses. *Earth and Planetary Science Letters*, 19, 290-300, 1973.

[40] Miyashiro A. Volcanic rock series in island arcs and active continental margins. *American Journal of Science*, 274, 321-355, 1974.

[41] Evensen, N.M., Hamilton, P.J. and O'Nions, R.K. Rare earth abundances in chondritic meteorites. *Geochemical and Cosmochemical Acta*, 4, 1199-1212,1978.

[42] Thompson, R.N., Morrisson, M.A., Hendry, G.L. and Parry, S.J. An assessment of the relative role of crust and mantle in magma genesis. An element approach. *Philosophic Transaction Royal Society London*, A 310, 549-590, 1984.

[43] Ama Salah, I., Liegeois, J.P. and Pouclet, A. Evolution d'un arc insulaire océanique birimien précoce au Liptako nigérian (Sirba): géologie, géochronologie et géochimie. *Journal of African Earth Sciences*, 22 (3), 235-254, 1996.

[44] Ayuso, R. and Arth, J.G. The Northeast Kingdom batholith, Vermon: magmatic evolution and geochemical constraints on the origin of Acadian granitic rocks. *Contribution to Mineralogy and Petrology*, 111 (1), 1-23, 1992.

[45] Bertrand, J.M., Dupuy, C., Dostal, J. and Davidson, I. Geochemistry and geotectonic interpretation of granitoids from Central Iforas (Mali, West Africa). *Precambrian Research*, 26 (3-4), 265-283, 1984.

[46] Chebeu, C., Ngo Nlend, C.D., Nzenti, J.P. and Ganno, S. Neoproterozoic High-K Calc-alcaline granitoids from Bapa-Batié, North Equatorial Fold Belt, Central Cameroon: petrogenesis and geodynamic significance. *The Open Geology Journal*, 4, 112-131, 2011.

[47] Djouka-Fonkwe, M.L., Schulz, B., Tchouankoué, J.P., and Nzolang, C. Geochemistry of the Bafoussam Pan-African I- and S-type granitoids in western Cameroon. *Journal of African Earth Sciences*, 50, 148-167, 2008.

[48] Duarte, B.P., Valente, S.C. and Campos Neto, M.C. Petrogenesis of the orthogneisses of the Mantiqueira Complex, Central Ribeira Belt, SE Brazil: an Archean to basement unit reworked during the Pan-African orogeny. *Gondwana Research*, 7, 437-450, 2004.

[49] Ferré, E.C., Déléris, J., Bouchez, J.L., Lar, A.U. and Peucat, J.J. The Pan-African reactivation of contrasted Eburnean and Archaean provinces in Nigeria: structural and isotopic data. *Journal of the Geological Society of London*, 153, 719-728, 1996.

[50] Ferré, E.C., Caby, R., Peucat, J.J., Capdevila, R. and Monié, P. Pan-African, postcollisional, ferro-potassic granite and quartz-monzonite plutons of Eastern Nigeria. *Lithos*, 45, 255-279, 1998.

[51] Heilbron, M., Machado, R. and Figueiredo, M. Lithogeochemistry of the Paleoproterozoic Granulites of the Bom Jardim de Minas (MG) Vassouras (RJ) Region, Central Segment of Ribeira Belt. *Revista Brasileirade Geociências*, 27, 83-98, 1997.

[52] Heilbron, M., Duarte, B.P. and Nogueira, J.R. The Juiz de Fora complex of the Central Ribeira belt, SE Brazil: a segment of granulitic crust thrusted during the Pan-African. *Gondwana Research*, 1, 373-382, 1998.

[53] Nguiessi, TC., Nzenti, J.P., Nsifa, E.N., Tempier, P. and Tchoua, F.M. Les granitoïdes calco-alcalins, syn-cisaillement de Bandja dans la Chaîne Panafricaine Nord-Equatoriale au Cameroun. *Comptes Rendus de l'Académie des Sciences*, 325, 95-101, 1997.

[54] Nogueira, J.R., Choudhuri, A. Geotectonic models and geologic evolution of the high-grade gneiss terranes of Juiz de For a (MG), Brazil. *Revista Brasileira de Geociências*, 30, 169-173, 2000.

[55] Nzenti, J.P., Barbey, P., Bertrand, J.M.L. and Macaudière, J. La chaîne panafricaine au Cameroun: cherchons suture et modèle. *In S.G.F. édit., 15e réunion des Sciences de la Terre, Nancy, France*, 99, 1994.

[56] Nzenti J. P., Kapajika B., Worner G. and Lubala Ruananza, T. Synkinematic emplacement of granitoids in a pan-african shear zone in central Cameroon. *Journal of African Earth Sciences*, 45, 74-86, 2006.

[57] Nzenti J.P., Abaga B., Suh C.E., Nzolang C. Petrogenesis of peraluminous magmas from the Akum-Bamenda Massif, Pan-African Fold Belt, Cameroon. *International Geology Review*, iFirst, 1-29, 2010.

[58] Nzolang, C., Kagam, H., Nzenti, J.P. and Holtz, F. Geochemistry and preliminary Sr-Nd isotopic data on the Neoproterozoic granitoids from the Bantoum area, West Cameroon: evidence for a derivation from a paleoproterozoic to Archaean crust. *Polar Geosciences*, 16, 196-226, 2003.

[59] Tagne-Kamga, G. Petrogenesis of Neoproterozoic Ngondo plutonic complex (Cameroon West central Africa): a case of late collisional ferro-potassic magmatism. *Journal of African Earth Science*, 36, 149-171, 2003.

[60] Tanko Njiosseu, E.L., Nzenti, J.P., Njanko, T., Kapajika, B., Nedelec, A. New U-Pb Zircon ages from Tonga (Cameroon): coexisting Eburnean Transamazonien (2.1 Ga) and Pan-African (0.6 Ga) imprints. *Comptes Rendus de l'Académie des Sciences de Paris*, 337, 551-562, 2005.

[61] Nzina, N.A., Nzenti, J.P., Tanko Njiosseu, E.L., Ganno, S. and Ngnotue, T. Synkinematic ferro-potassic magmatism from the Mekwene-Njimafofire Foumban Massif, along the Foumban-Banyo shear zone in central domain of Cameroon Pan-African fold belt. *Journal of Geology and Mining Research*, 2 (6), 142-158, 2010.

[62] Le Bas, M.J., Le Maître, R.W., Streckeisen, A. and Zanettin, B. A chemical classification of volcanic rocks based on the total alkali-silica diagram. *Journal of Petrology*, 27, 745-750, 1986.

[63] Cox, K.G., Bell, J. D. and Pankhurst, R.J. The Interpretation of Igneous Rocks, George Allen & Unwin, London, United Kingdom 445 pp, 1979.

[64] Sylvester, P.J. Post-collisional alkaline granites. *Journal of Geology*, 97, 261-280, 1989.

[65] Bachelor, R.A., Bowden, P. Petrogenetic interpretation of granitoid rock series using multicationic parameters. *Chemical Geology*, 48, 43-55, 1985.

[66] Nzenti, J.P. Neoproterozoic alkaline metamorphic igneous rocks from the Pan-African North Equatorial fold belt (Yaounde, Cameroon): biotites and magnetite rich pyroxenites. *Journal of Africa Earth Sciences*, 26, 1, 37-47, 1998.

[67] Nzenti, J.P., Ngako, V., Kambou, R., Penaye, J., Bassahak, J. and Njel, O.V. Structures régionales de la chaîne panafricaine du Nord Cameroun. *Comptes Rendus de l'Académie des Sciences Paris*, 315, II, 209- 215, 1992.

[68] Nedelec A., Macaudiere J., Nzenti J. P., and Barbey P. Evolution structurale et métamorphisme des schistes de Mbalmayo (Cameroun). Informations pour la structure de la zone mobile panafricaine d'Afrique centrale au contact du craton du Congo. *Comptes Rendus de l'Académie des Sciences, Paris*, 303, II, 75-80, 1986.

[69] Penaye, J., Toteu, S.F., Michard, A., Van Schmus, W.R. and Nzenti, J.P. U/Pb and Sm/Nd preliminary geochronologic data on the Yaoundé series, Cameroon: reinterpretation of granulitic rock as the suture of the collision in the « Centrafricain » belt. *Comptes Rendus de l'Académie des Sciences, Paris*, 317, 789-794, 1993.

[70] McDonough, W.F. Constraints on the composition of the lithospheric mantle. *Earth Planetary Science Letters*, 101, 1-18, 1990.

[71] Heaman, L.M., Le Cheminant, A.N. and Rainbird, R.H. Nature and timing of Franklin igneous events, Canada: implications for a Late Proterozoic mantle plume and the brak-up of Laurentia. *Earth Planetary Science Letters*, 109, 117-131, 1992.

[72] Guiraud, R. and Bosworth, W. Senonian basin inversion and rejuvenation of rifting in Africa and Arabia: synthesis and implications to plate-scale tectonics, *Tectonophysics*, 282, 39-82, 1997.

[73] Porada, H. Pan-African rifting and orogenesis in southern to equatorial Africa and eastern Brazil. *Precambrian Research*, 44, 103-136, 1989.

[74] Maurin, J.C. and Guiraud, R. Basement control in the development of the Early Cretaceous West and Central African Rift System. *Tectonophysics*, 228, 81-95, 1993.

[75] Tembo, F., Kampunzu, A.B., and Porada, H. Tholeiitic magmatism associated with continental rifting in the Lufilian Fold Belt of Zambia. *Journal of African Earth Sciences*, 28 (2), 403-425, 1999.

[76] Ngounouno I., Déruelle B., Guiraud R., Vicat, J.P. Magmatisme tholéiitique et alcalin des demi-grabens crétacés de Mayo Oulo-Léré et de Babouri-Figuil (Nord du Cameroun-Sud du Tchad) en domaine d'extension continentale. *Comptes Rendus de l'Académie des Sciences Paris*, 333, 201-207, 2001.

[77] Vicat, J.P., Ngounouno, I. and Pouclet, A. Existence de dyke doléritiques anciens à composition de tholéiites continentale au sein de la province alcaline de la ligne du Cameroun. Implication sur le contexte géodynamique. *Comptes Rendus de l'Académie des Sciences Paris*, 332, 243-249, 2001.

[78] Tanko Njiosseu, E.L. Géologie de la région de Tonga dans la partie Sud du domaine centre de la chaîne au Cameroun: évolution métamorphique, géochimie et géochronologie. *Unpublished Ph. D thesis, University of Yaoundé 1*, 104 p., 2012.